Journal of Catalysis 257 (2008) 345–355

Contents lists available at ScienceDirect

Journal of Catalysis

www.elsevier.com/locate/jcat

Preparation of carbon nanotube-supported metal nanoparticles coated with silica layers

Sakae Takenaka [a,*], Takafumi Arike [a], Hideki Matsune [a], Eishi Tanabe [b], Masahiro Kishida [a,*]

[a] Department of Chemical Engineering, Graduate School of Engineering, Kyushu University, Moto-oka 744, Nishi-ku, Fukuoka 819-0395, Japan
[b] Western Hiroshima Prefecture Industrial Institute, Kagamiyama, Higashi-Hiroshima 739-0046, Japan

ARTICLE INFO

Article history:
Received 13 March 2008
Revised 10 May 2008
Accepted 13 May 2008
Available online 17 June 2008

Keywords:
Carbon nanotube
Metal nanoparticles
Carbon nanotube-supported metal particles
Silica coating

ABSTRACT

Carbon nanotube (CNT)-supported Pt metal (Pt/CNT) was covered with silica layers using hydrolysis of 3-aminopropyl-triethoxysilane (APTES) and/or tetraethoxysilane (TEOS). The hydrolysis of APTES resulted in a uniform coverage of Pt/CNT with silica layers, but the silica layers were very thin. Pt/CNT could be coated with silica layers of a few nanometers thickness by hydrolysis of TEOS, but the thickness was not uniform. In contrast, the successive hydrolysis of APTES and TEOS resulted in a uniform coverage of Pt/CNT with silica layers of a few nanometers thickness. Pt metal particles in silica-coated Pt/CNT adsorbed CO chemically despite uniform coverage of Pt metal particles with silica layers. Therefore, silica-coated Pt/CNT demonstrated high catalytic activity in methane combustion.

1. Introduction

Carbon nanotubes (CNTs) have attracted a great deal of interest since their discovery [1]. CNTs are expected to find use in various applications, including chemical sensors and catalysts in chemical reactions, due to their unique magnetic, electronic, and chemical properties. To use CNTs in some applications, their surface must be modified with another phase to form highly functionalized composites. These composites are frequently prepared by coating the outer surface of CNTs with a secondary phase with a high level of functionalization [2]. Composites of CNTs and metal nanoparticles are often used as catalysts; for example, in one such application, a CNT-supported Pt metal nanoparticle composite (Pt/CNT) is used as an electrocatalyst in proton-exchange membrane fuel cells (PEMFCs) [3–5]. The Pt/CNT cathode catalyst is reported to show higher activity in the reduction of oxygen in PEMFCs than traditional carbon black-supported Pt catalysts, which have been widely used in PEMFCs. In addition, Rh and Ru metal nanoparticles supported on CNT show excellent catalytic performance in the selective hydrogenation of α,β-unsaturated aldehydes to unsaturated alcohols, whereas α,β-unsaturated aldehydes are generally hydrogenated to saturated alcohols over metal catalysts supported on conventional carriers [6–9]. Modifying CNT surfaces is generally a challenging task, however, because they are rather inert chemically. Even if the CNT surfaces are successfully modified with a secondary phase, the added phase often aggregates easily because they may have only weak interactions with CNTs [10]. Thus, in certain instances, inhibiting the aggregation of the secondary phase on CNTs is necessary to make practical use of CNT-based composites.

In the present study, CNT-supported metal nanoparticles were uniformly coated with silica layers. This coating was expected to inhibit aggregation of the metal particles. In previous work, we studied the preparation of metal nanoparticle catalysts uniformly coated with silica [11–14]. The metal nanoparticles in the catalysts showed high durability to sintering at high temperatures because they were uniformly covered with silica layers. In addition, we demonstrated that the silica-coated metal nanoparticle catalysts showed high catalytic activity despite the uniform coverage of metal nanoparticles with silica layers; for example, silica-coated Pt metal nanoparticles catalyzed the combustion of light alkanes, such as methane, ethane, propane, and butanes [13]. In addition, silica-coated Ni metal nanoparticles demonstrated high catalytic activity and high stability for the partial oxidation of methane into synthesis gas [14]. The coating of CNT surfaces with silica layers has been reported by many research groups [15–21]; however, to the best of our knowledge, very few reports have been published describing the coating of metal nanoparticles supported on CNTs with silica layers. The surface of silica-coated CNTs can be easily functionalized using one of the many chemical methods available for modification of silica surfaces. We believe that the coverage of CNT-supported metal nanoparticle composites with silica layers will permit their use in novel applications, such as catalytic reactions carried out under severe conditions, like elevated temperatures. Consequently, in the present study, Ru, Rh, and Pt metal nanoparticles supported on CNTs were coated with silica layers by

* Corresponding authors. Fax: +81 92 802 2752.
E-mail address: takenaka@chem-eng.kyushu-u.ac.jp (S. Takenaka).

0021-9517/$ – see front matter
doi:10.1016/j.jcat.2008.05.016

the successive hydrolysis of 3-aminopropyl-triethoxysilane (APTES) and tetraethoxysilane (TEOS). In addition, the CNT-supported metal nanoparticles covered with silica layers were used as catalysts in the combustion of methane to demonstrate their catalytic activity.

2. Experimental

2.1. Preparation of CNT-supported metal nanoparticles coated with silica layers

Commercially available CNTs (supplied from Ardrich; 20–30 nm o.d.; 5–10 nm i.d.; 0.5–200 μm long; >95% purity; 120 $m^2\,g^{-1}$ BET surface area) were immersed in an aqueous solution of H_2SO_4 and HNO_3. The solution was mixed ultrasonically at 328 K for 2 h to oxidize the CNT surface [4]. Oxidized CNTs were immersed in an aqueous solution containing H_2PtCl_6. After this treatment, the pH value of this solution was adjusted to ca. 11 by adding aqueous NH_3 to deposit some Pt metal precursors on the CNTs. After this solution was filtered, the samples were dispersed in a stirred solution of ethanol and water, and then aqueous NH_3 and either APTES or TEOS were added into the solution. The resulting mixture was stirred at 333 K for 1.5 h. In the case of the successive hydrolysis of APTES and TEOS, APTES and aqueous NH_3 were added to the solution containing CNT-supported Pt precursors, and the resulting mixture was stirred at 333 K for 0.5 h. Then hydrolysis of TEOS was performed in this solution at 333 K for 1 h. Finally, each sample was dried at 333 K in air, followed by exposure to an atmosphere of H_2 at 623 K for 3 h. The silica-covered Pt/CNT sample prepared from APTES alone and that prepared from TEOS alone were designated SiO_2/Pt/CNT-A and SiO_2/Pt/CNT-T, respectively. The sample prepared by the successive hydrolysis of APTES and TEOS was designated SiO_2/Pt/CNT-AT.

CNT-supported Ru or Rh metal particles also were covered with silica layers by the successive hydrolysis of APTES and TEOS, with $RuCl_3$ and $RhCl_3$ used as metal sources for their preparation. First, the CNTs were immersed in an aqueous solution containing $RuCl_3$ or $RhCl_3$. After this treatment, the pH value of this solution was adjusted to ca. 11 by addition of aqueous NH_3 to deposit Ru or Rh precursors on the CNTs. APTES and aqueous NH_3, followed by TEOS, were added to the solution containing the CNTs. This solution was filtered, and the sample thus obtained was dried at 333 K in air, then exposed to an atmosphere of H_2 at 623 K for 3 h. The CNT-supported Ru and Rh metal nanoparticles coated with silica layers were designate SiO_2/Ru/CNT-AT and SiO_2/Rh/CNT-AT, respectively.

2.2. Characterization of the samples

The content of metals (Ru, Rh, and Pt) and SiO_2 in the CNT-supported metal nanoparticles covered with silica layers was evaluated by X-ray fluorescence spectroscopy (XRF). The samples were ground into a fine powder and spread evenly on the polyethylene terephthalate film. The CNT content in CNT-supported metal nanoparticles covered with silica layers was evaluated by the thermogravimetric analysis in air. The samples were heated to 1173 K in an air stream, which resulted in the combustion of the CNTs.

Transmission electron microscopy (TEM) images of the samples were recorded with a JEOL JEM-3000F instrument. The catalyst samples reduced with hydrogen at 623 K were dispersed in isopropanol and the solution was mixed ultrasonically at room temperature. A part of this solution was dropped on the grid for the measurement of TEM images.

Measurements of X-ray absorption near-edge structure (XANES) and extended X-ray absorption fine structure (EXAFS) were performed at Photon Factory in the Institute of Materials Structure Science for High Energy Accelerator Research Organization, Japan (proposal 2007G532). XANES/EXAFS spectra were measured in a transmission mode at room temperature at beam line NW-10A with a Si(311) double-crystal monochromator for Ru and Rh K-edge absorption, and at beam line BL-9C with a Si(111) double-crystal monochromator for Pt L_{III}-edge absorption. The catalyst samples were reduced with hydrogen at 623 K before the measurement of XANES and EXAFS. The catalyst samples were packed in a polyethylene bag under an Ar atmosphere. The EXAFS data were analyzed using the REX EXAFS analysis program (Rigaku Co.). Fourier transformation of k^3-weighted EXAFS oscillations was performed over the k range of 3.5 to 15.5 $Å^{-1}$. Inversely Fourier transformed data for Fourier peaks were analyzed by a curve-fitting method using the phase shift and amplitude function derived from FEFF 8.0 [22].

Exposed surface areas of Pt metal particles in silica-coated Pt/CNT were evaluated by the CO adsorption method at 323 K, assuming an adsorption stoichiometry of 1:1 for CO/Pt. Before the measurement of CO adsorption, the samples were treated with hydrogen at 623 K for 30 min.

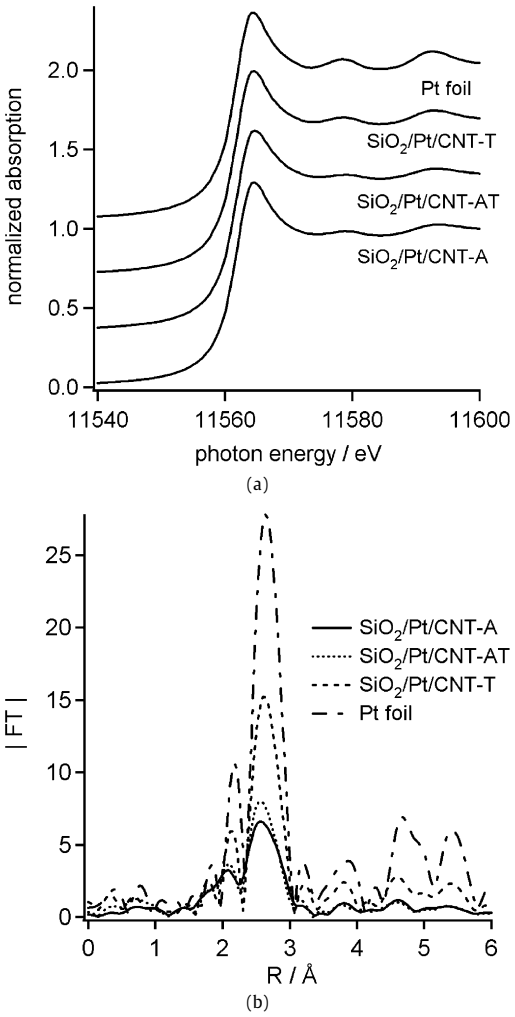

Fig. 1. Pt L_{III}-edge XANES spectra (a) and Fourier transforms of k^3-weighted EXAFS (b) for different SiO_2/Pt/CNT samples and Pt foil.

Table 1
Contents of Pt, SiO_2 and CNT in different SiO_2/Pt/CNT samples

Sample	Concentration ($mol\,l^{-1}$)		Content (wt%)		
	APTES	TEOS	Pt	SiO_2	CNT
SiO_2/Pt/CNT-A	0.041	–	6.2	7.3	86.5
SiO_2/Pt/CNT-T	–	0.041	5.5	31.2	63.3
SiO_2/Pt/CNT-AT	0.014	0.041	3.8	47.7	48.5

3. Results

3.1. Coverage of Pt/CNT with silica layers

Pt/CNT covered with silica layers was prepared by the hydrolysis of APTES and/or TEOS in the presence of CNT-supported Pt metal precursors, followed by the reduction of the resulting products with hydrogen at 623 K. Table 1 presents the SiO_2, Pt, and CNT contents in various SiO_2/Pt/CNT samples prepared in the present study, along with the concentrations of APTES and TEOS used in the preparation of each sample. Only a very small amount of SiO_2 was found on the surface of SiO_2/Pt/CNT-A, whereas a large amount of SiO_2 was contained in SiO_2/Pt/CNT-T and SiO_2/Pt/CNT-AT. Hydrolysis and polycondensation of APTES to form silica precursors do not occur readily, due to strong bonding between Si atoms and the 3-aminopropyl group, whereas TEOS is readily hydrolyzed to form silica precursors under the conditions used in the present study. Thus, the hydrolysis of APTES alone resulted in the deposition of a small amount of silica on Pt/CNT.

Fig. 1 shows Pt L_{III}-edge XANES spectra (a) and Fourier transforms of k^3-weighted EXAFS spectra [RSFs, radial structural functions; (b)] for SiO_2/Pt/CNT-A, SiO_2/Pt/CNT-T, SiO_2/Pt/CNT-AT, and Pt foil. The features of XANES spectra of all of the SiO_2/Pt/CNT samples were consistent with the XANES spectrum recorded using Pt foil. Moreover, the RSFs for all of the SiO_2/Pt/CNT samples were very similar in shape to that obtained for Pt foil, although peak in-

Table 2
Structural parameters of Pt species in different SiO_2/Pt/CNT samples estimated by curve-fitting analyses of EXAFS spectra

Sample	Shell	CN[a]	R (Å)[b]	DW (Å)[c]
SiO_2/Pt/CNT-A	Pt–Pt	7.6 (±0.3)	2.73	0.085
SiO_2/Pt/CNT-T	Pt–Pt	9.6 (±0.4)	2.75	0.070
SiO_2/Pt/CNT-AT	Pt–Pt	7.8 (±0.6)	2.73	0.083

[a] Coordination number.
[b] Interatomic distance.
[c] Debye–Waller factor.

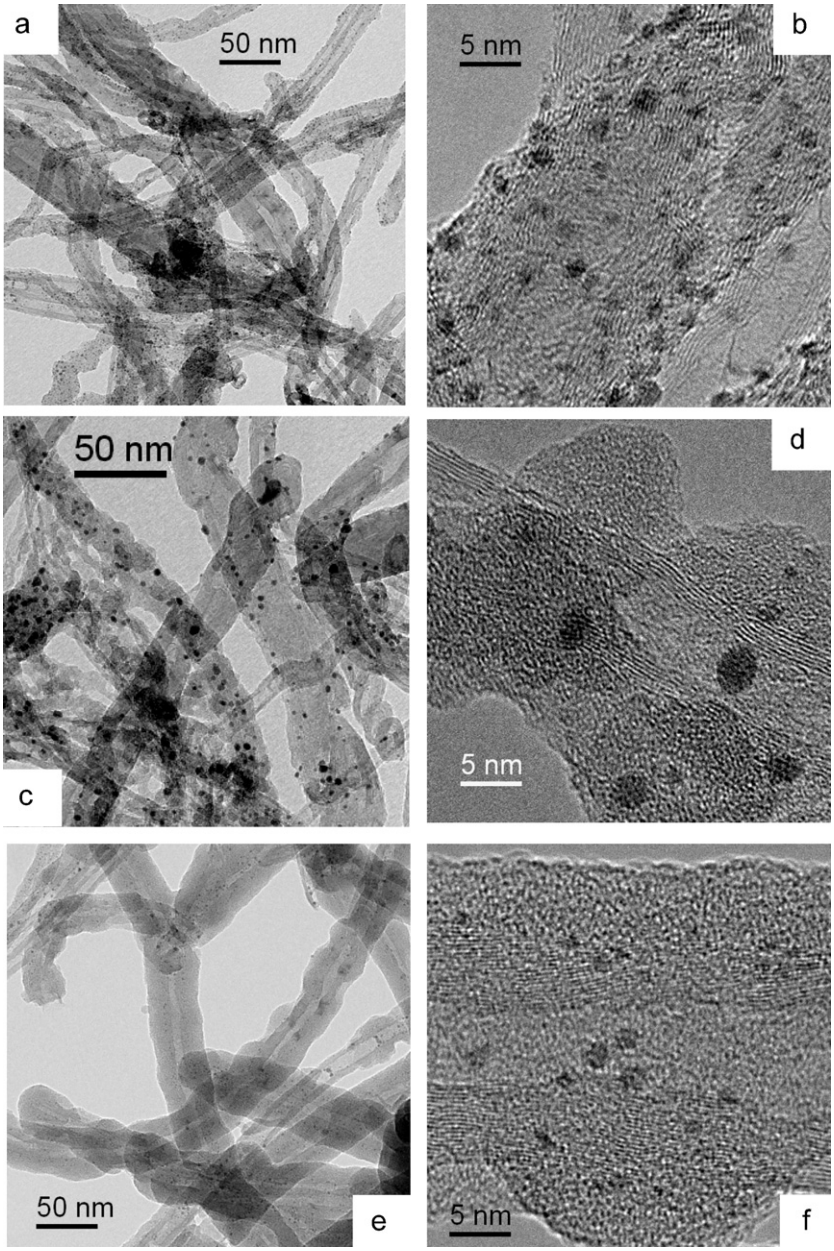

Fig. 2. TEM images of SiO_2/Pt/CNT-A (a and b), SiO_2/Pt/CNT-T (c and d) and SiO_2/Pt/CNT-AT (e and f).

tensities were strongly dependent on the type of sample. Thus, Pt species in all of the SiO_2/Pt/CNT samples were present as Pt metal. The peak at around 2.7 Å in the RSFs for all the SiO_2/Pt/CNT can be assigned to the first Pt–Pt shell in Pt metal on the basis of the RSF for Pt foil. The peak intensity in RSFs for any metal is directly proportional to its crystallite size [23,24]. The peak intensity due to Pt–Pt bond was the highest in the RSF of SiO_2/Pt/CNT-T compared with the peak intensities in the RSFs of SiO_2/Pt/CNT-A and SiO_2/Pt/CNT-AT. These results suggest that the average Pt particle size was the largest in SiO_2/Pt/CNT-T.

The peaks observed at around 2.7 Å in the RSFs of the SiO_2/Pt/CNT samples were inversely Fourier-transformed, and the EXAFS spectra thus obtained were fitted using the phase-shift and amplitude functions for Pt–Pt bonds. The results are given in Table 2. The EXAFS spectra for all of the SiO_2/Pt/CNT samples could be fitted by a Pt–Pt shell. The estimated coordination numbers of the Pt–Pt bond were 7.6 in SiO_2/Pt/CNT-A, 7.8 in SiO_2/Pt/CNT-AT, and 9.6 in SiO_2/Pt/CNT-T. Thus, the average crystallite size of Pt metal in SiO_2/Pt/CNT-T was larger than those in the other samples.

Fig. 2 shows TEM images of various SiO_2/Pt/CNT samples after reduction with hydrogen at 623 K. An average particle size of Pt metal in the samples was evaluated using these TEM images. In addition, specific surface areas of Pt metal particles in these samples were also evaluated using the particle size distribution of Pt metal estimated by these TEM images. These results are given in Table 3. TEM images (a) and (b) for SiO_2/Pt/CNT-A clearly show that Pt metal particles were supported on the outer surface of CNTs. The Pt metal particles had a diameter of 1–3 nm and a very narrow size distribution. Therefore, the preparation of SiO_2/Pt/CNT by the hydrolysis of APTES alone provided homogeneously dispersed Pt metal particles on these CNTs. However, the presence of silica layers in SiO_2/Pt/CNT-A could not be established from the TEM images of this sample. In contrast to the TEM images, energy-dispersive X-ray fluorescence (EDX) spectra, measured at the same time as the corresponding TEM images for SiO_2/Pt/CNT-A, demonstrated the presence of silica on the surface of SiO_2/Pt/CNT-A. Fig. 3 shows a TEM image for SiO_2/Pt/CNT-A as well as the elemental mapping for carbon and silicon atoms in the sample examined by EDX. It can be seen that silicon atoms were uniformly distributed on the outer surface of SiO_2/Pt/CNT-A. Therefore, the hydrolysis of APTES resulted in the uniform coverage of the Pt/CNT surface with very thin silica layers. In contrast, as shown in the TEM images (c) and (d) in Fig. 2, thick silica layers appeared to envelop the Pt metal particles and coat the surface of the SiO_2/Pt/CNT-T sample. However, the thickness of the silica layer in SiO_2/Pt/CNT-T was not uniform, and exposed CNT surfaces could be seen in the TEM images. Therefore, the hydrolysis of TEOS led to an irregular silica layer coating on the CNT surfaces. The Pt metal particles in SiO_2/Pt/CNT-T ranged in diameter from 1 to 6 nm, a broader size distribution than that seen in SiO_2/Pt/CNT-A. Remarkably, the successive hydrolysis of APTES followed by TEOS provided the SiO_2/Pt/CNT-AT sample with a smoother outer surface compared with that of SiO_2/Pt/CNT-T. As shown in the TEM images (e) and (f) in Fig. 2, the surface of SiO_2/Pt/CNT-AT was uniformly covered with thick silica layers. The diameter of the Pt metal particles in SiO_2/Pt/CNT-AT ranged from 1 to 3 nm, very similar to that for SiO_2/Pt/CNT-A. It is important to note that Pt metal particles in SiO_2/Pt/CNT-AT were found not on the outer surface of the silica layers, but rather in their bodies; therefore, the surfaces of Pt metal particles supported on CNT can be uniformly covered with silica layers by the successive hydrolysis of APTES and TEOS.

The SiO_2/Pt/CNT-AT sample was calcined at 1073 K under an air stream to examine whether the CNTs and Pt metal particles in the sample were covered with silica layers. Fig. 4 shows TEM images for calcined SiO_2/Pt/CNT-AT. These TEM images show the formation of silica tubes [15–21] with channel diameters of ca. 20 nm, similar to the outer diameter of the CNTs used in the present study. In addition, Pt metal particles with diameters ranging from 5 to 8 nm were always present in the channel of the silica tubes. When SiO_2/Pt/CNT-AT was calcined at 1073 K in air, the CNTs were oxidized completely to form silica tubes, and Pt metal particles, which had been supported on CNTs, aggregated in the channel of the silica tubes. These findings also strongly suggest that the entire surface of SiO_2/Pt/CNT-AT was uniformly covered with silica layers.

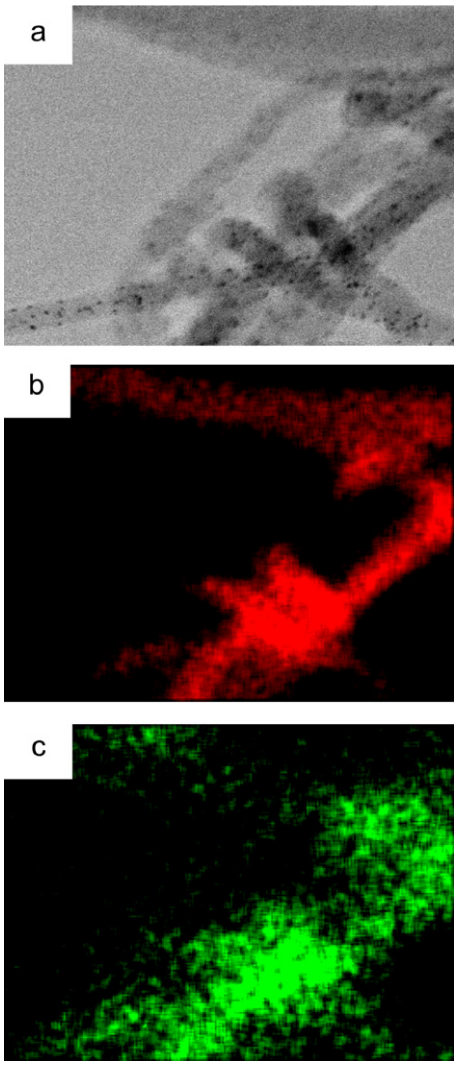

Fig. 3. TEM image of SiO_2/Pt/CNT-A (a), and elemental mapping for carbon atoms (b) and silicon atoms (c) examined by EDX for the sample.

Table 3
An average particle size and surface area of Pt metal in SiO_2/Pt/CNT-A, SiO_2/Pt/CNT-T and SiO_2/Pt/CNT-AT treated at different temperatures

Sample	Temp.[a] (K)	d (TEM)[b] (nm)	S (TEM)[c] (m^2 g-Pt^{-1})	S (CO)[d] (m^2 g-Pt^{-1})
SiO_2/Pt/CNT-A	623	1.7 ± 0.5	166	94
SiO_2/Pt/CNT-A	873	2.5 ± 0.9	116	75
SiO_2/Pt/CNT-T	623	2.9 ± 0.9	104	41
SiO_2/Pt/CNT-T	873	3.2 ± 1.2	93	34
SiO_2/Pt/CNT-AT	623	1.7 ± 0.5	173	111
SiO_2/Pt/CNT-AT	873	1.9 ± 0.5	163	90

[a] Temperature of the pretreatment for the samples.
[b] An average particle size of Pt metal estimated by TEM images of each SiO_2/Pt/CNT.
[c] Specific surface area of Pt metal particles estimated using particle size distribution of Pt metal which was evaluated by the TEM images.
[d] Exposed surface area of Pt metal particles estimated by CO adsorption methods.

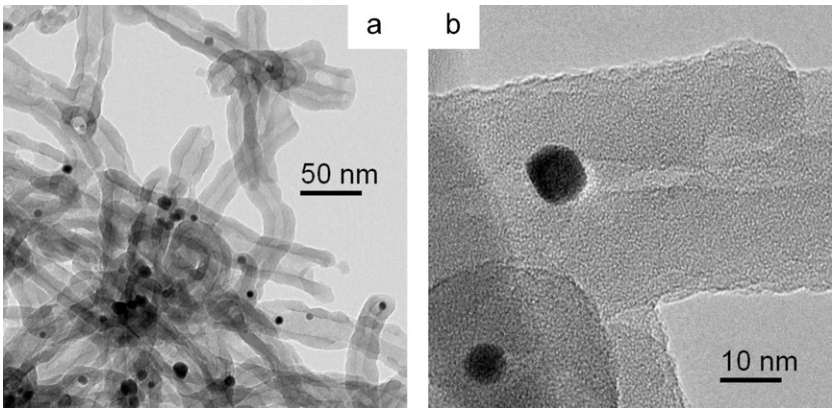

Fig. 4. TEM images of SiO_2/Pt/CNT-AT calcined under an air stream at 1073 K.

Table 4
Contents of Pt, SiO_2 and CNT in different SiO_2/Pt/CNT-AT samples

Entry	Concentration (mol l^{-1})		Content (wt%)		
	APTES	TEOS	Pt	SiO_2	CNT
1	0.014	0.014	4.4	26.3	69.3
2	0.014	0.041	3.8	47.7	48.5
3	0.041	0.550	2.1	77.5	20.4

The TEOS concentrations were varied to control the thickness of silica layers in the SiO_2/Pt/CNT-AT samples. Table 4 gives the concentrations of APTES and TEOS during sample preparation, along with the final SiO_2, Pt, and CNT content in each sample. Fig. 5 shows TEM images for these SiO_2/Pt/CNT-AT samples; panels (a) and (b), (c) and (d), and (e) and (f) correspond to the samples of entry 1, entry, 2 and entry 3 in Table 4, respectively. The TEM images for all of the SiO_2/Pt/CNT-AT samples in Fig. 5 show that the CNTs and Pt metal particles were uniformly coated with silica layers. The diameter of the Pt metal particles was very similar in all of the SiO_2/Pt/CNT-AT samples. In contrast, the thickness of silica layers in the SiO_2/Pt/CNT-AT samples was strongly dependent on the TEOS concentration; that is, the thickness of silica layers increased from 2 nm to 5 nm by changing the TEOS concentration from 0.014 to 0.041 mol l^{-1}. When the TEOS concentration was further increased to 0.550 mol l^{-1}, the silica layers grew to ca. 15 nm thick, as shown in the TEM images (e) and (f) in Fig. 5. As described earlier, the hydrolysis of APTES on the CNTs did not contribute to the formation of thick silica layers. This finding indicates that the thickness of silica layers that envelop Pt/CNT can be controlled by varying the TEOS concentration during their preparation.

3.2. Coverage of CNT-supported Ru and Rh with silica layers

CNT-supported Ru and Rh metal nanoparticles also were covered with silica layers by the successive hydrolysis of APTES and TEOS. Fig. 6 shows Ru K-edge XANES spectra (a) and RSFs (b) for SiO_2/Ru/CNT-AT, Ru metal powder, and RuO_2. The Ru K-edge XANES spectrum for Ru metal powder differed in shape from that for RuO_2; that is, the absorption at around 22140 eV for RuO_2 (white line) was stronger than that at around 22120 eV for Ru metal, and the threshold of absorption at around 22105 eV for Ru metal was of lower energy compared with that for RuO_2. Thus, the XANES spectra provide useful information on the oxidation state of Ru species [25,26]. The XANES spectrum for SiO_2/Ru/CNT-AT showed more similarity with that of Ru metal than with that of RuO_2; however, the threshold of XANES spectrum at around 22105 eV for SiO_2/Ru/CNT-AT was at slightly higher energy compared with that for Ru metal. Furthermore, the intensity of absorption at around 22120 eV for SiO_2/Ru/CNT-AT was slightly higher than that for Ru metal. These results reveal that some Ru species in the SiO_2/Ru/CNT-AT sample existed in the oxidized state, although most of the Ru species were present as Ru metal. The RSFs in Fig. 6b also suggest that Ru species in SiO_2/Ru/CNT-AT were present as both Ru metal and Ru oxides. In the RSF for SiO_2/Ru/CNT-AT, a strong peak was observed at around 2.3 Å in addition to a small peak at around 1.7 Å. Based on the analysis of the XANES spectra and the RSFs for RuO_2 and Ru metal powder, the peaks at 2.3 Å and 1.7 Å can be assigned to Ru–Ru bonds in Ru metal and Ru–O bonds in Ru oxides, respectively. The intensity of the peak due to Ru–Ru bond in SiO_2/Ru/CNT-AT was significantly lower than the peak intensity for Ru metal powder, suggesting a very small average crystallite size of Ru metal in SiO_2/Ru/CNT-AT.

To further clarify the structure of Ru species in SiO_2/Ru/CNT-AT, curve-fitting analysis of its EXAFS spectrum was performed. The peaks in the RSF were inversely Fourier-transformed in the R range of 0.5–3.0 Å, and the EXAFS spectrum thus obtained was fitted in the k range of 4.0–15.0 $Å^{-1}$. The results are given in Table 5. The EXAFS spectrum for SiO_2/Ru/CNT-AT could be fitted by a shell of the Ru–O bond and a shell of the Ru–Ru bond. The low coordination number of the Ru–Ru bond suggests the presence of Ru metal with small crystallite size in SiO_2/Ru/CNT-AT. The Ru metal particles in the sample likely interacted strongly with the silica layers, as indicated by the small crystallite size of Ru metal; the fraction of the surface Ru atoms in Ru metal particles should be higher with a smaller crystallite size of Ru. The surface Ru atoms in Ru metal particles in SiO_2/Ru/CNT-AT directly interact with silica layers through Si–O–Ru bonds; therefore, some Ru species in the sample could exist in the oxidized state.

Fig. 7 shows Rh K-edge XANES spectra (a) and RSFs (b) for SiO_2/Rh/CNT-AT and Rh foil. The XANES spectrum for SiO_2/Rh/CNT-AT was consistent with that recorded with Rh foil. In addition, the RSF for SiO_2/Rh/CNT-AT also was similar in shape to that for Rh foil, even though the peak intensity was significantly lower in the former sample. The structural parameters of Rh species estimated by curve-fitting analysis of the EXAFS spectrum for SiO_2/Rh/CNT-AT are given in Table 5. The peak in the RSF was inversely Fourier-transformed in the R range of 1.0–3.0 Å, and the EXAFS spectrum thus obtained was fitted in the k range of 4.0–15.0 $Å^{-1}$. The EXAFS spectrum for SiO_2/Rh/CNT-AT could be fitted only by a shell of the Rh–Rh bond due to Rh metal; thus, we can conclude that Rh species in SiO_2/Rh/CNT-AT were present as Rh metal.

Fig. 8 shows TEM images of SiO_2/Ru/CNT-AT (a and b) and SiO_2/Rh/CNT-AT (c and d). The TEM images for both of the silica-coated samples show CNTs and metal particles covered uniformly with silica layers of a few nanometers thickness. In addition, the metal particles in these samples range in size from 1 to 3 nm and have a very narrow distribution. Thus, homogeneously dispersed

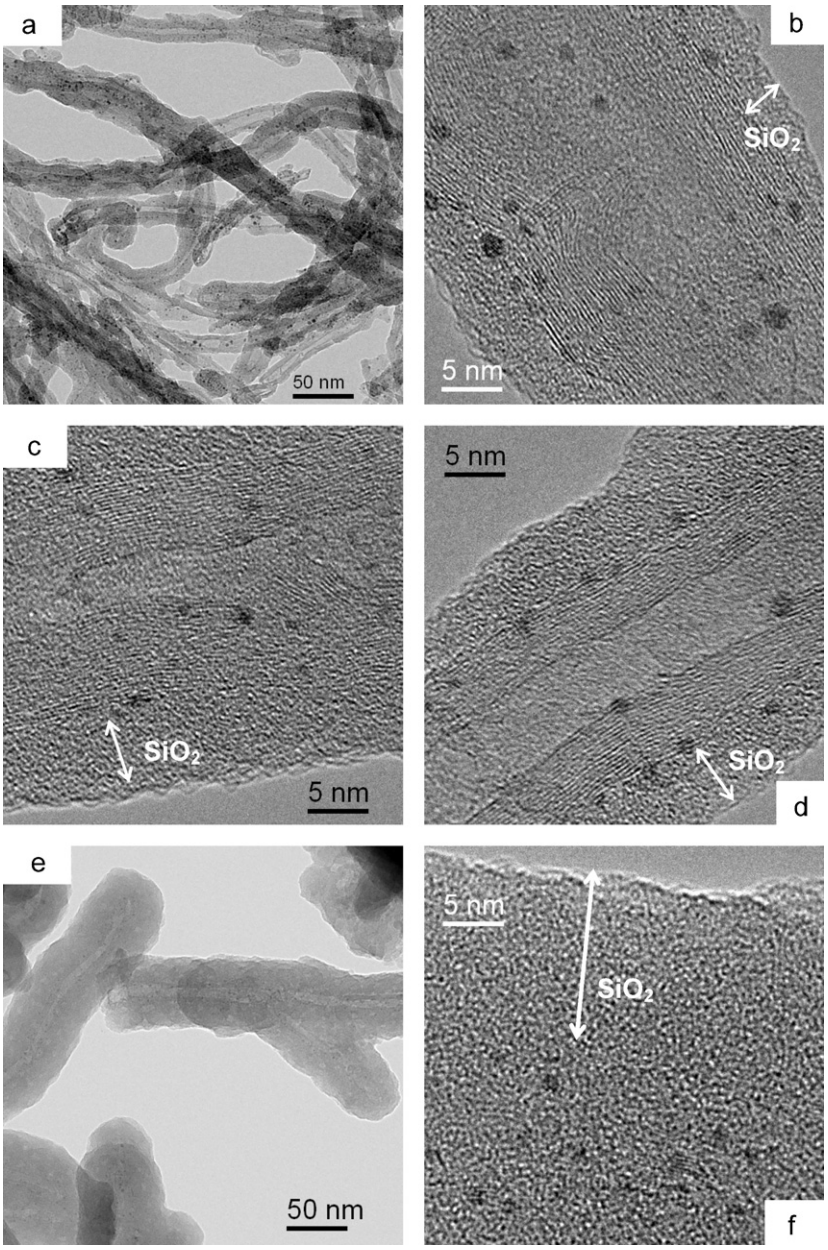

Fig. 5. TEM images of SiO_2/Pt/CNT-AT prepared using different concentrations of APTES and TEOS.

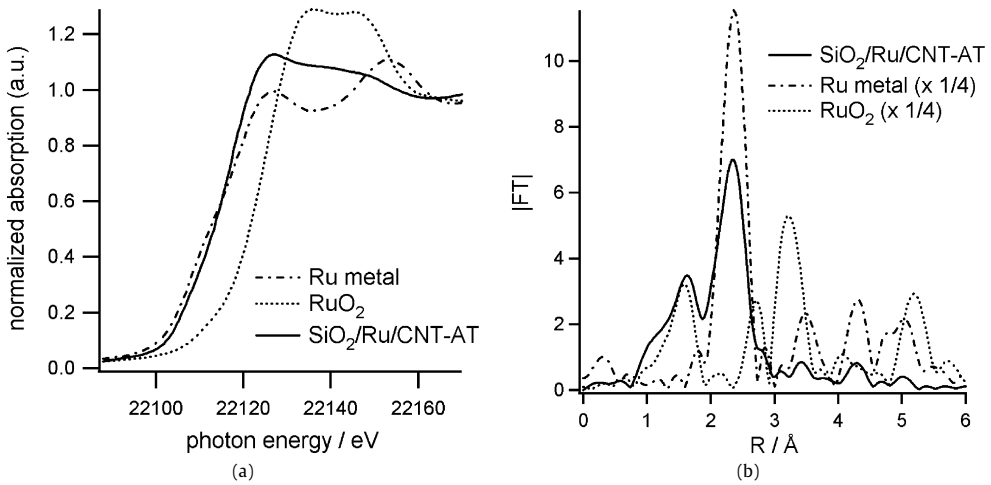

Fig. 6. Ru K-edge XANES spectra (a) and Fourier transforms of k^3-weighted EXAFS spectra (b) for SiO_2/Ru/CNT-AT, Ru metal powder and RuO_2. Intensities of the peaks in the RSFs for Ru metal powder and RuO_2 were reduced by quarter.

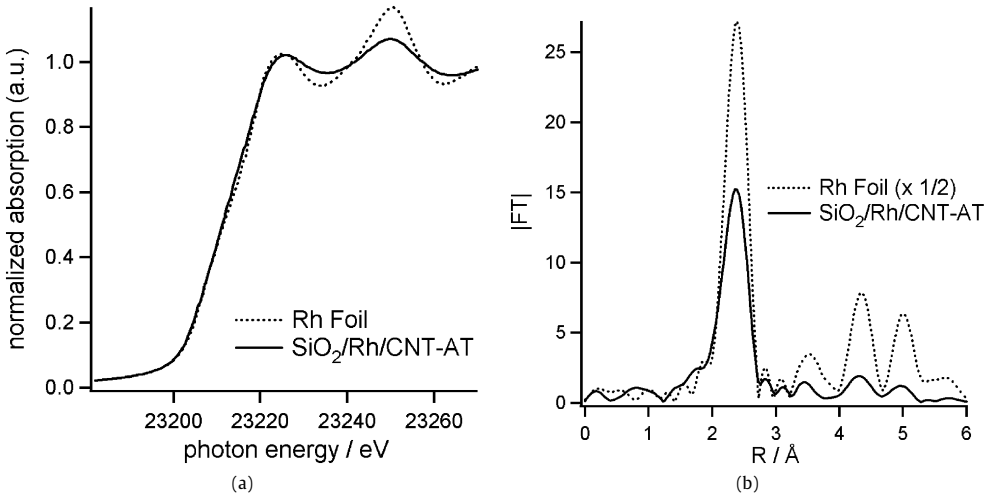

Fig. 7. Rh K-edge XANES spectra (a) and Fourier transforms of k^3-weighted EXAFS spectra (b) for SiO_2/Rh/CNT-AT and Rh foil. Intensities of the peaks in the RSF for Rh foil were reduced by half.

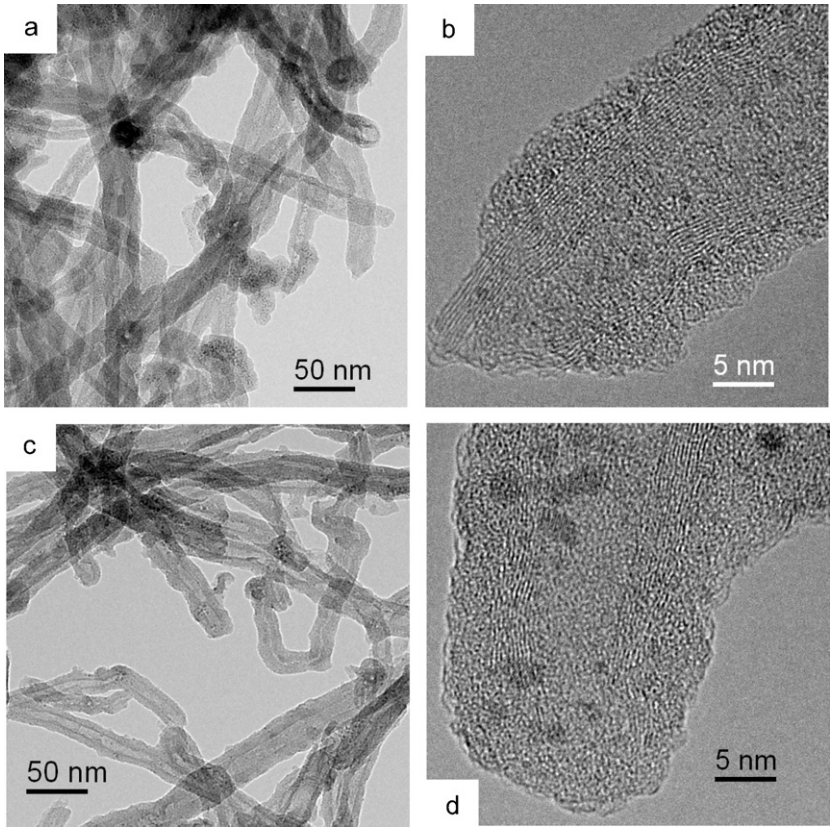

Fig. 8. TEM images of SiO_2/Ru/CNT-AT (a and b) and SiO_2/Rh/CNT-AT (c and d).

Table 5
Structural parameters of metal species in SiO_2/Ru/CNT-AT and SiO_2/Rh/CNT-AT estimated by curve-fitting analyses of the EXAFS spectra

Sample	Shell	CN[a]	R (Å)[b]	DW (Å)[c]
SiO_2/Ru/CNT-AT	Ru–O	1.8 ± 0.4	1.99	0.075
	Ru–Ru	4.0 ± 0.4	2.64	0.088
SiO_2/Rh/CNT-AT	Rh–Rh	6.2 ± 0.3	2.67	0.077

[a] Coordination number.
[b] Interatomic distance.
[c] Debye–Waller factor.

Rh and Ru metal nanoparticles supported on CNT can be covered uniformly with silica layers by the successive hydrolysis of APTES and TEOS.

3.3. Catalytic performance of SiO_2/Pt/CNT

As described earlier, CNT-supported metal nanoparticles could be covered uniformly with silica layers by the successive hydrolysis of APTES and TEOS. The silica layers that coat metal nanoparticles may potentially prevent the chemical adsorption of small molecules, such as CO and hydrogen, on metal surfaces. To investigate whether the catalytic activity of the metal nanoparticles is affected by the silica coating, CO adsorption experiments using SiO_2/Pt/CNT samples were carried out. Based on the amount of CO adsorbed on the samples, an exposed surface area of Pt metal particles was estimated. Before the adsorption of CO at 323 K, these samples were treated with hydrogen at 623 K for

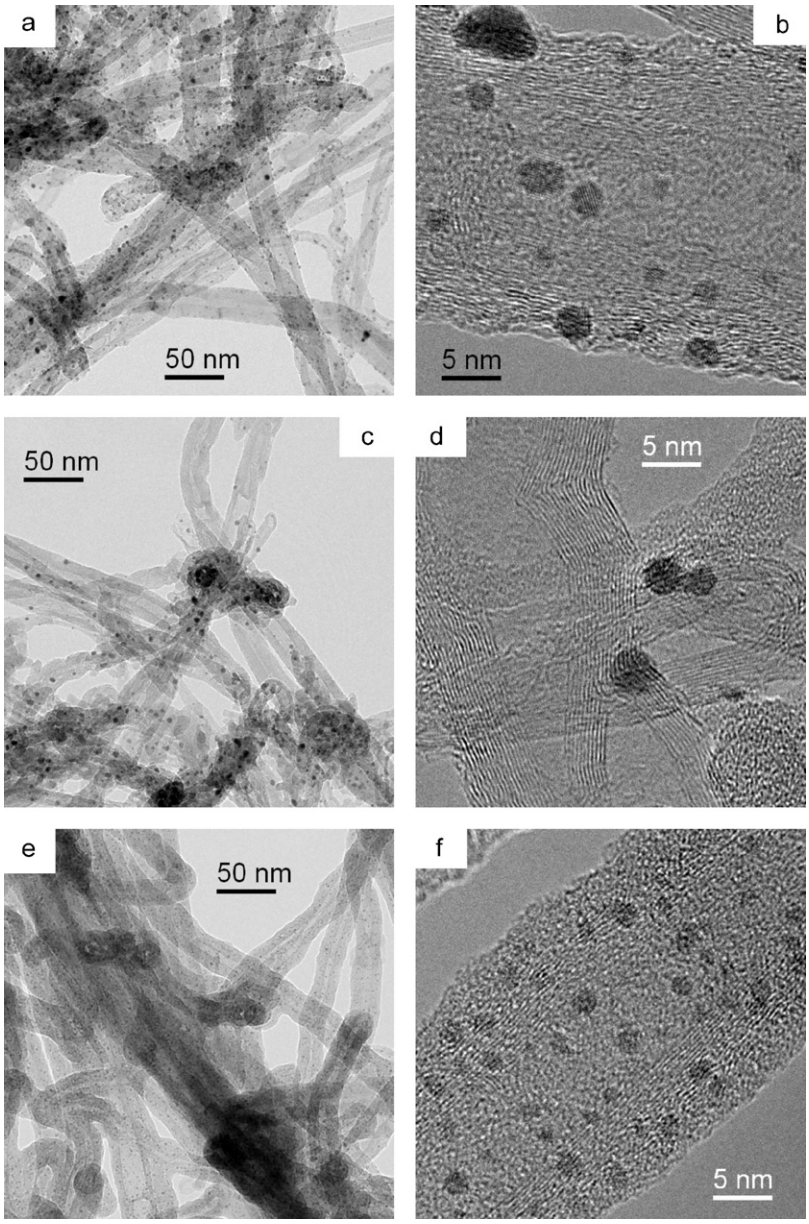

Fig. 9. TEM images of SiO_2/Pt/CNT-A (a and b), SiO_2/Pt/CNT-T (c and d) and SiO_2/Pt/CNT-AT (e and f) treated at 873 K in a stream of Ar.

30 min. In addition, to examine tolerance to sintering of Pt metal particles in these samples, the samples were exposed to 873 K in an atmosphere of Ar for 5 h, then to 623 K in an atmosphere of hydrogen for 30 min. Fig. 9 shows the TEM images of SiO_2/Pt/CNT-A, SiO_2/Pt/CNT-T, and SiO_2/Pt/CNT-AT treated at 873 K in Ar. Table 3 gives the exposed surface areas of Pt metal particles in the samples treated at 873 K, evaluated by the amount of CO adsorbed. The exposed surface area of Pt metal, estimated by CO adsorption methods, was 94 $m^2\,g^{-1}$ for SiO_2/Pt/CNT-A, 41 $m^2\,g^{-1}$ for SiO_2/Pt/CNT-T, and 111 $m^2\,g^{-1}$ for SiO_2/Pt/CNT-AT after the treatment with hydrogen at 623 K. The exposed surface areas of Pt metal particles estimated by CO adsorption methods for all of the SiO_2/Pt/CNT were smaller than the specific surface areas of Pt metal particles estimated based on TEM images of the corresponding samples, due to the coverage of Pt metal particles with silica layers. Keep in mind, however, that the Pt metal surface in SiO_2/Pt/CNT-AT was highly exposed. On the other hand, the exposed surface areas of the Pt metal particles in the SiO_2/Pt/CNT estimated by CO adsorption decreased slightly after the samples were treated at 873 K under Ar. TEM images of the SiO_2/Pt/CNT revealed an increase in the average size of the Pt metal particles after the samples were treated at 873 K under Ar, as shown in Fig. 9, in which the increment in average particle size of the Pt metal in SiO_2/Pt/CNT-A is especially noticeable. Therefore, the decrease in exposed surface areas of Pt metal particles in SiO_2/Pt/CNT after the treatment at 873 K should be due to the sintering of Pt metal particles. However, the decreases in average particle size and exposed surface area of Pt metal in SiO_2/Pt/CNT-AT were more insignificant than those in SiO_2/Pt/CNT-A and SiO_2/Pt/CNT-T. These findings suggest that the uniform coverage of Pt metal particles with silica layers of a few nanometers in thickness improved the resistance to sintering of Pt metal particles on CNT.

Methane combustion was performed over Pt/CNT, SiO_2/Pt/CNT-AT, and Pt/SiO_2 to clarify the effect of silica coating on the catalytic performance of Pt/CNT. In reactions carried out over all of the catalysts, complete oxidation of methane occurred to form CO_2 and H_2O. Fig. 10 shows the changes in turnover frequency (TOF) val-

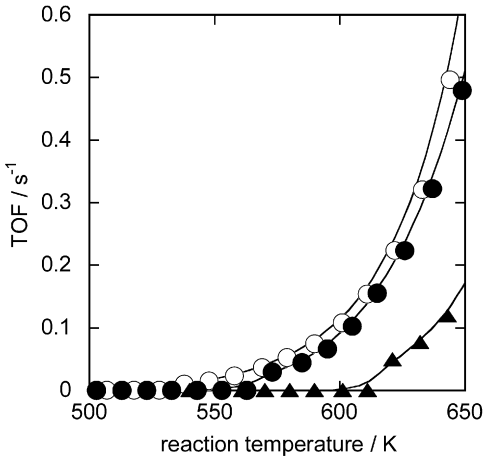

Fig. 10. Change in TOF values with reaction temperatures in the methane combustion over Pt/CNT (●), SiO_2/Pt/CNT-AT (○) and Pt/SiO_2 (▲). $P(CH_4) = 18.0$ kPa, $P(O_2) = 16.0$ kPa, $P(He) = 67.3$ kPa, flow rate = 75 ml min^{-1}.

ues with increasing reaction temperatures in methane combustion. Based on the amount of CO adsorbed on these catalysts, TOF values in methane combustion were estimated, assuming that the number of active sites available for the combustion of methane was equivalent to the number of CO molecules adsorbed on Pt metal particles. The TOF values for SiO_2/Pt/CNT-AT were very similar to those for Pt/CNT, even though the catalytic activity of Pt/SiO_2 was slightly lower than that of the other catalysts. These findings clearly demonstrate that the coverage of Pt metal particles with silica layers did not decrease their catalytic activity.

4. Discussion

CNT-supported Pt metal particles covered with silica layers were prepared using the hydrolysis of TEOS or APTES, followed by the successive hydrolysis of APTES and TEOS. In the hydrolysis of TEOS on the CNTs, silica precursors should be formed by homogeneous nucleation through the hydrolysis of TEOS, with the small particles of silica precursors deposited on the outer surface of the CNTs to form silica layers. In the successive hydrolysis of APTES and TEOS on CNTs, APTES are adsorbed densely on the outer surface of CNT through strong interactions between the graphene sheets of CNTs and the amino group of APTES [16]. The APTES adsorbed on the CNTs is hydrolyzed to form the thin layers of silica precursors on the CNTs. In the subsequent hydrolysis of TEOS on the CNTs covered with silica precursors from APTES, silica precursors from TEOS should be formed by heterogeneous nucleation and be deposited on the CNTs, because the silica precursors from APTES act as nucleation sites of silica precursors from TEOS. The heterogeneous nucleation of silica precursors from TEOS would form layers with a high density on the CNTs compared with homogeneous nucleation. In addition, the chemical interaction between the silica precursors from TEOS and the silica precursors from APTES on the CNTs should be stronger than that between the silica precursors from TEOS and the bare CNT surfaces. In fact, exposed CNT surfaces were seen in the TEM images of SiO_2/Pt/CNT-T after the treatment at 623 K (Figs. 2c and 2d), even though the CNT surface in SiO_2/Pt/CNT-AT was uniformly covered with silica layers. It should be noted that most of the silica layers in SiO_2/Pt/CNT-T peeled off after exposure to 873 K, whereas the Pt metal particles and CNTs remained uniformly covered with silica layers in the SiO_2/Pt/CNT-AT samples exposed to 873 K, as shown in Fig. 9. These results imply that silica layers formed from TEOS only are fragile at high temperatures. Silica precursors from TEOS formed by homogeneous nucleation were deposited coarsely on the bare CNT surfaces, resulting in the formation of silica layers that readily peel off at high temperatures. In addition, it should be noted that Pt metal particles in SiO_2/Pt/CNT-AT were smaller than those in SiO_2/Pt/CNT-T, as clarified by the TEM images in Fig. 2. In the preparation of SiO_2/Pt/CNT-AT, Pt precursors on the CNTs formed by the addition of aqueous NH_3 to aqueous H_2PtCl_6 were surrounded by dense silica precursor layers formed by the hydrolysis of APTES, due to the strong interaction between APTES and CNT. The silica precursors on the CNT formed from APTES should prevent the sintering of Pt metal particles during reduction of the Pt precursors with hydrogen at 573 K. Thus, the Pt metal particles in SiO_2/Pt/CNT-AT should be smaller than those in SiO_2/Pt/CNT-T.

The present study has demonstrated that Pt metal particles in silica-coated Pt/CNT chemically adsorbed CO despite uniform coverage of Pt metal particles with silica layers. Thus, silica-coated Pt/CNT demonstrated high activity for methane combustion, as shown in Fig. 10. The silica layers that enveloped the Pt/CNT should be composed of the aggregates of small silica particles. Small molecules, such as CO and methane, likely are supplied to the surfaces of Pt metal particles in silica-coated Pt/CNT through the porous structure of the silica layers (i.e., through the spaces between the small silica particles). The Pt metal particles in silica-coated Pt/CNT would weakly interact with the silica particles, because the Pt L_{III}-edge XANES spectra of silica-coated Pt/CNT were very similar to those recorded with Pt foil. Thus, silica-coated Pt/CNT demonstrated high catalytic activity, irrespective of the coverage of Pt metal with silica layers.

As described earlier, Pt metal particles in all of the SiO_2/Pt/CNT samples, especially SiO_2/Pt/CNT-A and SiO_2/Pt/CNT-AT, were very small and homogeneous in size. These SiO_2/Pt/CNT samples were prepared by the hydrolysis of APTES and/or TEOS in the presence of CNT-supported Pt metal precursors, which were formed through

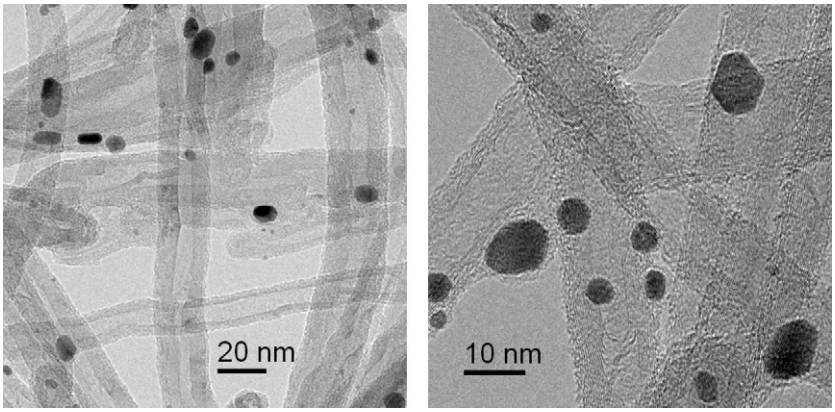

Fig. 11. TEM images of Pt/CNT prepared by the reduction of CNT-supported Pt precursors with hydrogen at 623 K.

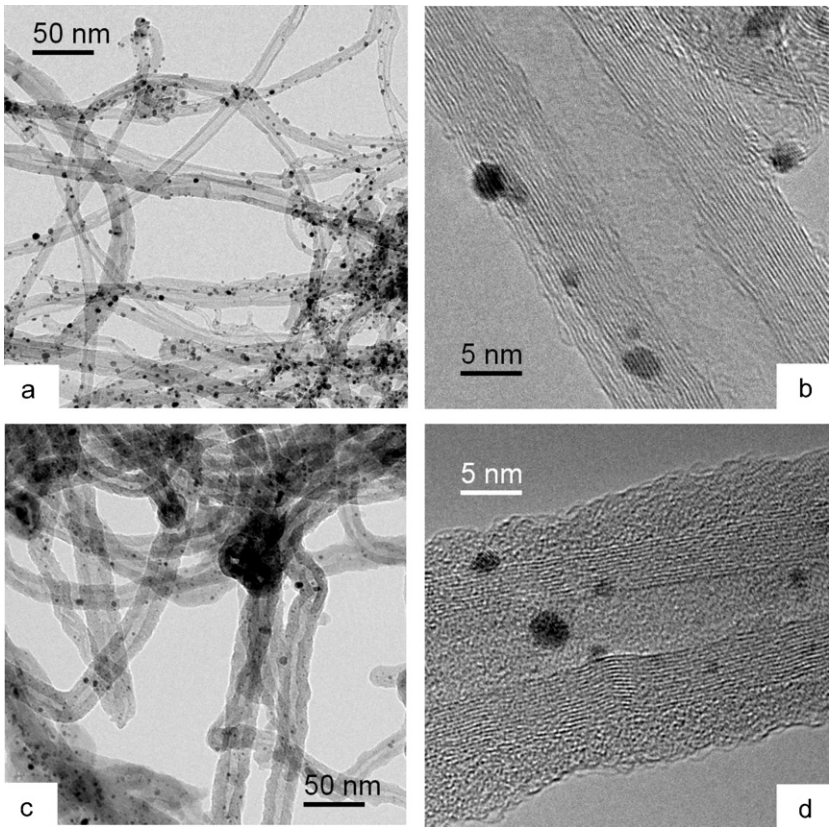

Fig. 12. TEM images of Pt/CNT (a and b) and Pt/CNT covered with silica layers (c and d).

the addition of aqueous NH_3 to aqueous H_2PtCl_6. Reduction of the Pt precursors on the CNT surface likely would result in small, homogeneous Pt metal particles. To test this theory, CNT-supported Pt metal particles without silica coating were prepared by the reduction of CNT-supported Pt precursors with hydrogen at 623 K. Fig. 11 shows TEM images of Pt/CNT thus obtained, demonstrating Pt metal particles ranging in diameters from 2 to 10 nm, a very broad diameter distribution. Thus, it can be concluded that preparation of Pt metal by the reduction of Pt precursors formed by the addition of aqueous NH_3 to aqueous H_2PtCl_6 did not contribute to the small size and homogeneous dispersion of Pt metal particles.

CNT-supported Pt metal particles covered with silica layers also could be prepared by the successive hydrolysis of APTES and TEOS using CNT-supported Pt metal particles, instead of CNT-supported Pt metal precursors. Fig. 12 shows TEM images of Pt/CNT before and after coating with silica layers. Pt/CNT was prepared by impregnation of CNT in an alcoholic solution containing H_2PtCl_6, followed by reduction with hydrogen at 623 K. Figs. 12a and 12b show Pt metal particles ranging in diameter from 1 to 4 nm on the outer CNT surface of the Pt/CNT sample before silica coating. After the successive hydrolysis of APTES and TEOS in the presence of the Pt/CNT, followed by the treatment of the resulting products with hydrogen at 623 K, the outer surfaces of Pt metal particles and CNTs appeared to be uniformly covered with silica layers (Figs. 12c and 12d). The Pt metal particles in Pt/CNT covered with silica layers were similar in diameter to those in Pt/CNT; however, the Pt metal particles in the Pt/CNT covered with silica layers were larger than those in SiO_2/Pt/CNT-AT, which was prepared from Pt metal precursors supported on CNT (Figs. 2e and 12f). In general, controlling the size of metal particles on the supports by a conventional impregnation method is difficult, because metal particles are readily aggregated during reduction of metal precursors at high temperatures. In contrast, Pt metal precursors were reduced to Pt metal after coating with silica precursor layers in the preparation of SiO_2/Pt/CNT-AT, and the aggregation of Pt metal particles was not observed. The silica precursor layers enveloping Pt metal precursors should prevent the aggregation of Pt metal particles during reduction with hydrogen at 623 K. The high dispersion of Pt metal particles on the catalytic supports is a desirable property, because Pt is one of the most expensive metals. The preparation of SiO_2/Pt/CNT by the successive hydrolysis of APTES and TEOS using Pt metal precursors supported on CNT is an effective method for the deposition of smaller Pt metal particles on CNT.

5. Conclusion

The present paper reports the preparation of the CNT-supported metal nanoparticles covered with silica layers using the successive hydrolysis of APTES and TEOS in the presence of the corresponding metal precursors supported on CNTs, followed by reduction of the resulting products with hydrogen at 623 K. The thickness of silica layers can be controlled by varying the concentration of TEOS during preparation of the silica-coated samples. The coating of CNT-supported metal nanoparticles with silica layers improves the resistance to sintering of metal particles at high temperatures, but does not prevent significant chemical adsorption of small molecules, such as CO, on the metal surfaces. These findings suggest that CNT-supported metal nanoparticles covered with silica layers can be used as catalysts in catalytic reactions even at high temperatures.

Acknowledgments

This study was supported by the Industrial Technology Research Grant Program in 2005 from the New Energy and Industrial Technology Development Organization (NEDO) of Japan.

References

[1] S. Iijima, Nature 354 (1991) 56.
[2] P. Serp, M. Corrias, P. Kalck, Appl. Catal. A Gen. 253 (2003) 337.
[3] Z. Liu, X. Lin, J.Y. Lee, W. Zhang, M. Han, L.M. Gan, Langmuir 18 (2002) 4054.
[4] Y. Xing, J. Phys. Chem. B 108 (2004) 19255.
[5] N. Rajalakshmi, H. Ryu, M.M. Shaijumon, S. Ramaprabhu, J. Power Sources 140 (2005) 250.
[6] J.M. Planeix, N. Coustel, B. Coq, V. Brotons, P.S. Kumbhar, R. Dutartre, P. Geneste, P. Bernier, P.M. Ajayan, J. Am. Chem. Soc. 116 (1994) 7935.
[7] V. Lordi, N. Yao, J. Wei, Chem. Mater. 13 (2001) 733.
[8] J.P. Tessonnier, L. Pesant, G. Ehret, M.J. Ledoux, C. Pham-Huu, Appl. Catal. A Gen. 288 (2005) 203.
[9] H. Vu, F. Gonçalves, R. Philippe, E. Lamouroux, M. Corrias, Y. Kihn, D. Plee, P. Kalck, P. Serp, J. Catal. 240 (2006) 18.
[10] Y.T. Kim, K. Ohshima, K. Higashimine, T. Uruga, M. Takata, H. Suematsu, T. Mitani, Angew. Chem. Int. Ed. 45 (2006) 407.
[11] T. Tago, T. Hatsuta, K. Miyajima, M. Kishida, S. Tashiro, K. Wakabayashi, J. Am. Ceram. Soc. 85 (2002) 2188.
[12] S. Takenaka, Y. Orita, E. Tanabe, H. Matsune, M. Kishida, J. Phys. Chem. C 111 (2007) 7748.
[13] S. Takenaka, K. Hori, H. Matsune, M. Kishida, Chem. Lett. 34 (2005) 1594.
[14] S. Takenaka, H. Umebayashi, E. Tanabe, H. Matsune, M. Kishida, J. Catal. 245 (2007) 392.
[15] T. Seeger, Ph. Redlich, N. Grobert, M. Terrones, D.R.M. Walton, H.W. Kroto, M. Rühle, Chem. Phys. Lett. 339 (2001) 41.
[16] Q. Fu, C. Lu, J. Liu, Nano Lett. 2 (2002) 329.
[17] E.A. Whitsitt, A.R. Barron, Nano Lett. 3 (2003) 775.
[18] A.B. Bourlinos, V. Georgakilas, R. Zboril, P. Dallas, Carbon 45 (2007) 2136.
[19] H.W. Kim, S.H. Shim, J.W. Lee, Carbon 45 (2007) 2695.
[20] H. Ogihara, M. Sadakane, Y. Nodasaka, W. Ueda, Chem. Mater. 18 (2006) 4981.
[21] I. Kiricsi, Á. Fudala, Z. Kónya, K. Hernádi, P. Lentz, J.B. Nagy, Appl. Catal. A Gen. 203 (2000) L1.
[22] A.L. Ankudinov, B. Ravel, J.J. Rehr, S.D. Conradson, Phys. Rev. B 58 (1998) 7565.
[23] R.B. Greegor, F.W. Lytle, J. Catal. 63 (1980) 476.
[24] S.D. Jackson, J. Willis, G.D. McLellan, G. Webb, M.B.T. Keegan, R.B. Moyes, S. Simpson, P.B. Wells, R. Whyman, J. Catal. 139 (1993) 191.
[25] T. Tanaka, H. Yamashita, R. Tsuchitani, T. Funabiki, S. Yoshida, J. Chem. Soc. Faraday Trans. 1 (1989) 84, 2987.
[26] W.C. Ketchie, E.P. Maris, R.J. Davis, Chem. Mater. 19 (2007) 3406.